JOURNAL OF AIRCRAFT
Vol. 38, No. 3, May–June 2001

Applications of Zero-Net-Mass Jets for Enhanced Rotorcraft Aerodynamic Performance

Ahmed A. Hassan*
The Boeing Company, Mesa, Arizona 85205-3805

Numerical studies were conducted to investigate the beneficial effects of using arrays of zero-net-mass (ZNM) "synthetic" jets on the aerodynamic characteristics of the NACA-0012 airfoil. Flowfield predictions were made using modified versions of the NASA Ames ARC2D, U.S. Army 2DBVI unsteady, two-dimensional, compressible thin-layer Navier–Stokes flow solvers. An unsteady surface transpiration boundary condition was enforced over a user-specified portion of the airfoil's upper, or lower, surface to emulate the time variation of the mass flux out from and into the airfoil's surface. Special emphasis is placed on two-dimensional model problems that are representative of the more complex three-dimensional helicopter rotor flowfield environment. The numerical results have indicated that ZNM jets can be used to enhance the lift characteristics of airfoils (helicopter rotor blades) and alleviate the impulsive aerodynamic response of a helicopter blade during encounters with the tip vortex wake. The effectiveness of ZNM jets for aerodynamic control is shown to increase with the increase in freestream Mach number and, more importantly, with the decrease in the ratio between the peak jet Mach number to the freestream Mach number. The striking similarities with the aerodynamics of an airfoil having an array of surface protuberances are presented.

Introduction

WITH the recent advances in smart materials technology and the emergence of an array of microfabricated electromechanical systems (MEMS), it appears that a compliant-like aerodynamic surface (e.g., airfoil, wing, rotor blade, fuselage, etc.) may indeed be feasible. Potentially, these microsystems, or similar macrosystems which are based on the same principal of operation, can provide solutions that avert the use of more traditional complex mechanical, electrical, and pneumatic control systems for aerodynamic enhancement and control. For example, in the rotorcraft community the use of higher harmonic control of blade-root pitch[1] and the use of a blade-mounted trailing-edge flap[2] have been known to alleviate the impulsive aerodynamic response (and hence the acoustics) of rotor blade-vortex interactions (BVI). Moreover, the benefits of actively altering the effective leading-edge geometry and camber of a helicopter blade on rotor BVI were recently demonstrated[3] through numerical simulations involving the use of continuous (i.e., steady) normal, rather than tangential, surface blowing and the use of a combination of blowing and suction. These actuation methods, regardless of the control technique being utilized, typically require a "hub-based" complex control system (be it to actuate the rotor swash plate, to actuate the trailing-edge flap, or to administer air to the rotor blades).

From a practical rotor design point an "on-blade" control method that emulates the aerodynamic effects which result from blade-root pitch, from the deflection of the trailing-edge flap, and from steady surface blowing would, of course, be ideal because it eliminates the need for a hub-based complex control system. For example, the emulation of surface blowing without any actual mass transfer would also be very desirable because it eliminates the need for the air management system that administers the air to the blades in the rotating system.

Among the various MEMS designs, zero-net-mass or synthetic jets[4] appear to be the most promising where the potential for significant lift enhancement,[5] BVI noise reduction, and configuration drag reduction[5,6] appear to be the largest. In short, a zero-net-mass or synthetic jet results from oscillating a diaphragm in an enclosed rigid cavity having an orifice. Figure 1 is a sketch illustrating the general features of a zero-net-mass jet actuator. As perceived by an observer standing next to the exit port, periodic flow out of and into the cavity is seen. The boundary condition for the jet is therefore one that represents an oscillating velocity vector simply described using a harmonic function. Here, the synthesized external jet-like flow results from the entrainment of the surrounding ambient fluid as a result of the fluctuations in the pressure along the axis of the jet.

Typically, the diaphragm of a zero-net-mass actuator is activated electrostatically, electromagnetically, or through the use of a piezoelectric material with frequencies that span 1–14 kHz. The mechanics of the jet resemble those associated with the outward and inward flows observed when one moves a piston forward and backward in a cylinder having a single orifice. In general, air moves out of the cylinder when the piston is moved forward displacing the volume of air ahead of it. When the piston is moved backward, air is drawn into the cylinder by virtue of the low-level suction pressure created in the cylinder cavity. If the displaced volumes associated with the motion of the piston are equal, then the net-mass transfer across the port, for all practical purposes, is equal to zero (hence the name zero-net-mass jet). In recent laboratory tests conducted at the Boeing Company, peak jet velocities on the order of 185 ft/s at a frequency of 110 Hz were measured near the orifice of a first generation zero-net-mass electromagnetic actuator.

In this paper we present results from numerical simulations conducted using modified versions of the ARC2D (Ames Research Center two-dimensional)[7] and the U.S. Army 2DBVI (Two-dimensional blade-vortex interaction)[8] Navier–Stokes flow solvers to illustrate the beneficial aerodynamic effects, which result from the use of an array(s) of zero-net-mass jets (AZNMJ) on the surface of the NACA-0012 airfoil. Specifically, the following is demonstrated: 1) the improved lift capability of the airfoil (the basic element for a rotor blade or wing), 2) the favorable effects associated with the increase in freestream Mach number on the aerodynamics of the airfoil, and 3) the benefits of using two AZNMJ to alleviate the impulsive aerodynamic response of an airfoil during encounters with a line vortex (two-dimensional model problem for the more complex helicopter rotor parallel BVI problem). In the absence of experimental data on oscillatory transverse (i.e., acting in a direction normal to the aerodynamic surface and/or the free stream) jets, we revert to illustrating the striking similarities with the aerodynamics of an airfoil having an array of surface protuberances. Specifically, we will demonstrate

Presented as Paper 98-0211 at the 36th Aerospace Sciences Meeting, Reno, NV, 12–15 January 1998; received 8 April 1999; revision received 24 May 2000; accepted for publication 2 June 2000.

*Associate Technical Fellow, Computational Fluid Dynamics. Associate Fellow AIAA.

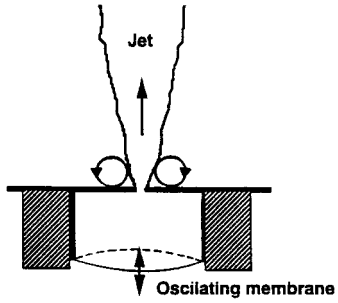

Fig. 1 Sketch of a zero-net-mass synthetic jet actuator.

that the behavior of the predicted lift and drag forces, in a mean sense, for an airfoil having an AZNMJ are quite similar to those arrived at from experimental data for an airfoil having an array of surface protuberances. To provide additional background for the present studies, we will refer, where applicable, to earlier results.[9]

Prediction Methods

For the baseline NACA-0012 airfoil and for the NACA-0012 airfoil with the AZNMJ, predictions were made using a modified version of the NASA Ames ARC2D Navier–Stokes flow solver.[7] This flow solver was selected among others because of its demonstrated accuracy in predicting the aerodynamic characteristics of helicopter rotor airfoils[10] and, in particular, the NACA-0012 airfoil. An alternating-direction-implicit approximate factorization scheme was used to solve the discretized equations on a body-fitted curvilinear grid. Second-order implicit and fourth-order explicit dissipation terms were added to the difference equations to improve stability and reduce solution oscillations in regions of large pressure gradients. Additional details relating to the solution algorithm can be found in Ref. 7.

For the airfoil-vortex interaction problem the "perturbation" approach by Srinivasan[8] was adopted. This approach was used by Baeder et al.[11] in their studies of the propagation of airfoil-vortex interaction noise. In the perturbation approach the dependent flow variables in the Navier–Stokes equations are decomposed into two parts. The first represents the perturbation caused solely by the flow past the airfoil, and the second represents the dependent variables associated with the embedded vortex (e.g., induced velocities). Using simple algebraic manipulation of the resulting Navier–Stokes equations, a similar set of governing equations are obtained for the unknown perturbation quantities. The numerical simulations of airfoil-vortex interactions with, and without, the AZNMJ included a Lamb vortex[8] located at an initial position equal to five airfoil chord lengths upstream of the airfoil's leading edge (i.e., $xv/C = -5.0$) and a distance equal to $0.25C$ below the airfoil (i.e., $zv/C = -0.25$). Here, C is the airfoil's chord length.

For a given jet-exit condition the interaction between the jet flow and the surrounding fluid can be simulated using a time-dependent boundary condition. As perceived by an observer standing next to the exit port, periodic flow out of and into the cavity is felt (see Fig. 1). The boundary condition for the jet is therefore one that represents an oscillating velocity vector described using a harmonic function. In this respect the modifications performed to both flow solvers entailed the enforcement of user-specified unsteady surface transpiration velocities only at the grid point locations that correspond to those of the AZNMJ. In the modified ARC2D and 2DBVI flow solvers the algebraic Baldwin–Lomax turbulence model[12] was used to compute the turbulent eddy viscosity.

All computations were performed on a C-type mesh having a resolution of 277×60 (100 points on each of the upper and lower surfaces of the airfoil; 39 points on each of the wake cuts, which extended from the airfoil's upper and lower surface trailing-edge points to the downstream outflow boundaries; and 60 points in the direction normal to the airfoil's surface). The NASA Ames hyperbolic grid generator HYGRID[13] was used to generate the computational grid while enforcing grid orthogonality at the surface of the airfoil. Grid clustering was performed near the surface of the airfoil to resolve the details of the boundary layer and the jet flow. In the computational grid the first grid points off the airfoil's surface were located at a distance equal to $0.00001C$ ensuring the presence of 12 grid planes in a y^+ value of 1.2. The far-field boundary was located at a distance approximately equal to sixteen airfoil chord lengths.

Surface Boundary Condition

The results presented here were obtained assuming that an array containing 10 zero-net-mass jets is placed on either the lower, the upper, or both surfaces of the NACA-0012 airfoil. In two of the examples presented, namely, the simulation of the aerodynamic effects that result from the use of a trailing-edge flap and the alleviation of the impulsive aerodynamic response associated with airfoil-vortex interactions, two (rather than one) AZNMJ are simulated. In these examples the two arrays are placed at identical chord positions on the upper and on the lower surfaces of the airfoil. Specifically, the array(s) of 10 jets extended over the airfoil's chord between the $x/C = 0.13$ and 0.23 nondimensional chord positions.

We assume that the normalized (by freestream speed of sound) oscillating jet velocity $q(t)$ can be described using a sinusoidal function of the form

$$q(t) = vn * \sin(2\Pi f t) \tag{1}$$

where vn represents the normalized (by the freestream speed of sound) amplitude of the peak blowing/suction velocity, f is the normalized (using airfoil chord and freestream velocity) frequency of the oscillation, and t is the nondimensional time (normalization factor is given by the ratio of the airfoil's chord length to the free stream speed of sound). In the analyses the sinusoidal boundary condition was enforced at each of the 10 user-defined grid nodes that collectively represented the AZNMJ. At all remaining surface grid points the no-slip viscous boundary condition was enforced. In the numerical simulations all jets were assumed to operate in unison with no phase shift. All jets were also assumed to have the same instantaneous velocity (or based on the adopted normalization, Mach number) given by Eq. (1). Figure 2 depicts the temporal variations of the prescribed jet velocities for three values of vn equal to 0.05, 0.10, and 0.20. The positive and negative jet velocities are associated with the blowing and the suction portions of the jet oscillation cycle, respectively.

Results and Discussion

All time-accurate predictions for the NACA-0012 airfoil were obtained using the ARC2D-predicted steady solution for the baseline airfoil (i.e., without the AZNMJ) as an initial starting solution. Table 1 depicts comparisons between the measured[14] and the ARC2D-predicted sectional lift C_L, drag C_D, and pitching-moment coefficients C_m for the baseline NACA-0012 airfoil at a freestream Mach number of 0.60, angles of attack α of 0 and 2 deg, and a Reynolds number of 3×10^6.

In Table 1 note that the ARC2D predictions are generally in good agreement with the measured sectional lift values. However, sectional drag and pitching-moment values are overpredicted.

In the flow control simulations the nondimensional timescale for one complete cycle involving blowing and suction was set equal

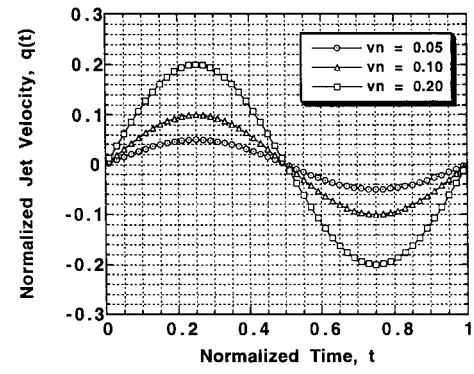

Fig. 2 Temporal variation of jet velocity.

Table 1 Predicted and measured aerodynamic characteristics for the baseline NACA-0012 airfoil

Method	α deg	C_L	C_D	C_m
Predicted	0	0	0.0098	0
Measured	0	0	0.0092	0
Predicted	2	0.2899	0.0106	0.0038
Measured	2	0.2824	0.0095	0.0031

to 1.0 with the nondimensional time step Δt being equal to 0.01. The computations for the airfoil-vortex interaction problem proceeded in a two-step procedure. In the first step we find the steady-state solution for a user-prescribed fixed initial vortex position (e.g., $xv/C = -5.0, zv/C = -0.25$). In the second step, using the steady-state solution found in step one as an initial condition, we compute the unsteady solution for the airfoil-vortex interaction problem where the vortex is left to convect freely by the local flow. When simulating the effects of the AZNMJ, only the second step is repeated while enforcing the unsteady transpiration boundary condition for the jets.

Unlike the problem for the NACA-0012 airfoil, the airfoil-vortex interaction problem involves two (rather than one) timescales. These are the timescale associated with the convection of the vortex and the timescale associated with the jet oscillation frequency. In the computations simulating the airfoil-vortex interaction problem, these two timescales were reduced to one, but not without difficulty, albeit a minor one. This difficulty is manifest in the need for a smaller time step (e.g., $\Delta t = 0.005$ rather than 0.01) to satisfy the numerical stability of the solver and, more importantly, to allow for the accurate simulation of the unsteady interactions between the airfoil/vortex/AZNMJ flowfields.

To demonstrate the effects of the AZNMJ on the aerodynamics of the NACA-0012 airfoil, the majority of the numerical simulations were performed for a freestream Mach number of 0.60 and an angle of attack of 0 deg. The choice of a zero angle of attack was intentionally made here so that we can illustrate the impact of the AZNMJ on the lift and pitching-moment values of the airfoil, which are, for these freestream conditions, known to be zero because of the geometric symmetry of the airfoil. Results for other angles of attack and jet oscillation frequencies can be found in Ref. 9. The effects of freestream Mach number, hence the effects of compressibility, on the aerodynamics of the airfoil for a freestream angle of attack of 0 deg are presented in the next section.

Use of AZNMJ for Lift Enhancement

Figure 3 depicts the effects of varying the jet peak velocity vn on the time histories of the predicted sectional lift for the NACA-0012 airfoil. In these simulations the freestream Mach number is 0.60, the angle of attack is 0 deg (i.e., a nonlifting case for the *baseline* NACA-0012 airfoil), and the Reynolds number based on the airfoil's chord length is 3×10^6. The results are shown for one AZNMJ located on the airfoil's lower surface between $x/C = 0.13$ and 0.23. In the predictions the jet oscillation frequency is 1585 Hz. Once the unsteady solutions reach a periodic state, the attained mean sectional lift values are seen to be equal to 0.06, 0.16, 0.38 for $vn = 0.05$, 0.10, and 0.20, respectively. It is shown that solution periodicity is achieved after approximately 13, 16, and 18 jet oscillation cycles for $vn = 0.05$, 0.10, and 0.20, respectively. In general, the results of Fig. 3 indicate that higher mean lift values are expected with the use of higher peak jet velocities and vice versa. Moreover, because of the symmetry of the NACA-0012 airfoil, if the AZNMJ is placed on the upper, rather than the lower, surface of the airfoil then one would expect the attained mean sectional lift values to be negative rather than positive.

The effects of the peak jet velocity vn on the temporal variations of the predicted sectional drag are shown in Fig. 4. The figure indicates that after achieving periodicity the attained mean drag values are equal to 0.011, 0.0140, and 0.027 for peak jet velocities equal to 0.05, 0.10, and 0.20, respectively. For the baseline airfoil the predicted sectional drag value is equal to 0.0098. In a given cycle

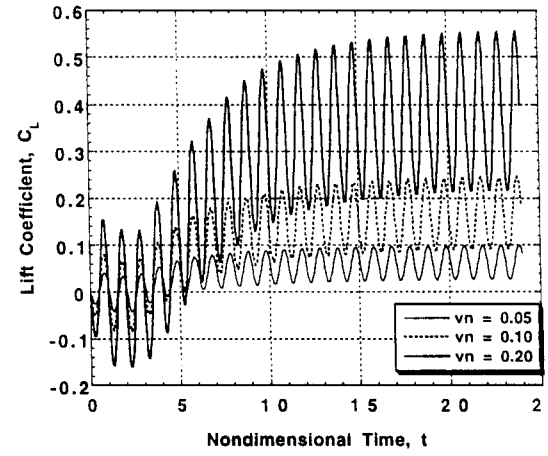

Fig. 3 Predicted time histories of the sectional lift for the NACA-0012 airfoil—effect of peak jet velocity vn ($M_{inf} = 0.6, \alpha = 0$ deg, $Re = 3 \times 10^6$, and $f = 1585$ Hz).

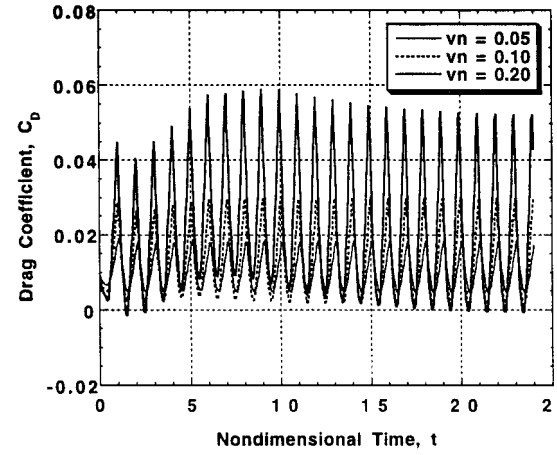

Fig. 4 Predicted time histories of the sectional drag for the NACA-0012 airfoil—effect of peak jet velocity ($M_{inf} = 0.6$, $\alpha = 0$ deg, $Re = 3 \times 10^6$, and $f = 1585$ Hz).

the magnitude of the maximum drag values are quite sensitive to the peak jet velocity vn. In contrast, smaller differences are seen between the minimum drag values for the three jet velocities considered. Therefore, the observed increase in the overall mean drag levels is primarily a result of the increase in the maximum, and not the minimum, drag values for the airfoil.

The results of Fig. 4 suggest that the minimum drag values decrease with the increase in the jet peak velocity. For example, whereas the minimum drag values are equal to 0.0048 for a peak jet velocity of 0.05 the minimum drag values are slightly negative (near zero) for a peak jet velocity of 0.20. In Ref. 9 it is shown that for a given jet oscillation frequency the minimum drag values are strongly dependent on the magnitude of the instantaneous jet velocity and the perceived adjustment of the duration of the blowing and the suction portions of the jet oscillation cycle. More precisely, as perceived by an observer near the exit of the jet and for angles of attack other than zero, say positive angles, the magnitude of the jet velocities during the blowing portion of the cycle are reduced by virtue of the y component (i.e., normal to the chord direction) of the freestream velocity. During the suction portion of the cycle, the opposite is true, as the magnitude of the jet velocities appear to increase. This apparent decrease and increase in the blowing and suction jet velocities result in a perceived asymmetric, rather than a symmetric, blowing/suction schedule (see Fig. 2). A similar plot that depicts the effects of varying the magnitude of the peak jet velocity on the time histories of the predicted pitching moments is shown in Fig. 5. The figure indicates that the attained mean pitching-moment values are equal to -0.011, -0.0235, and -0.033 for peak jet velocities

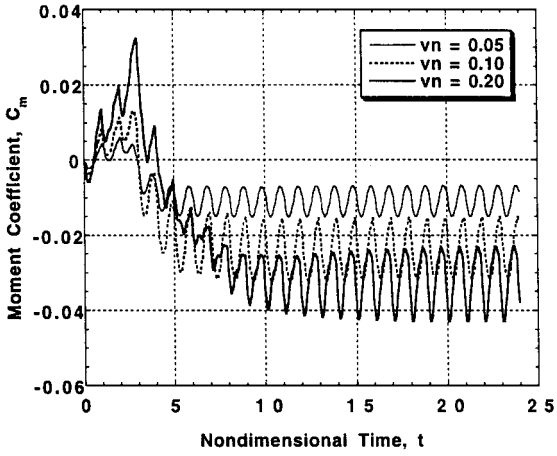

Fig. 5 Predicted time histories of the pitching moment for the NACA-0012 airfoil—effect of peak jet velocity (M_{inf} = 0.6, α = 0 deg, Re = 3 × 10^6, and f = 1585 Hz).

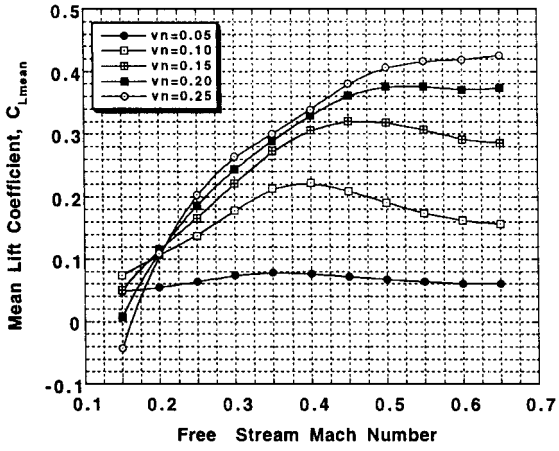

Fig. 6 Predicted mean sectional lift values for the NACA-0012 airfoil—effect of freestream Mach number (α = 0 deg, Re = 3 × 10^6, and f = 1585 Hz).

of 0.05, 0.10, and 0.20, respectively. The results of Fig. 5 indicate that higher mean pitching-moment values, in the absolute sense, are expected with the higher peak jet velocities and vice versa.

Effects of Freestream Mach Number

The effects of freestream Mach number, and hence the effects of compressibility, on the attained mean sectional lift values as a function of peak jet velocity vn are shown in Fig. 6. The results are shown for a freestream angle of attack of 0 deg. Large changes in the mean lift coefficients are only feasible at moderate-to-high subsonic Mach numbers. As seen, the effectiveness of the transverse zero-net-mass jets as a means to increase the airfoil's sectional lift is significantly reduced at the lower Mach numbers.

To explain the reason for the observed degradation in aerodynamic performance, we consider an alternate representation of the results shown in Fig. 6. Here, we elect to plot the attained mean sectional lift as a function of a Mach-number ratio (defined as the ratio between the jet Mach number vn or M_{jet} and the freestream Mach number M_{inf}) (see Fig. 7). Each of the curves correspond to a specific freestream Mach number, and the five points that constitute each of the curves correspond to peak jet velocities of 0.05, 0.10, 0.15, 0.20, and 0.25 respectively. For example, for a freestream Mach number of 0.15 and a peak jet velocity of 0.05 the Mach-number ratio is $\frac{1}{3}$. Referring to Fig. 7, we notice that for a freestream Mach number of 0.15 the predicted mean sectional lift values gradually increase reaching a maximum value of 0.074 at a Mach-number ratio of 0.667 (or a jet peak velocity vn of 0.10). For higher values of the Mach-number ratio, the predicted mean sectional lift values gradu-

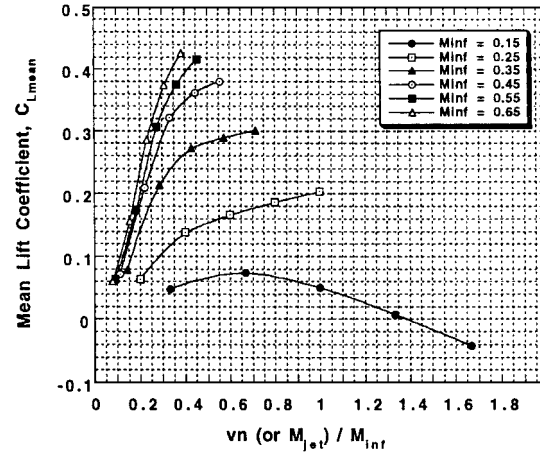

Fig. 7 Predicted mean sectional lift values for the NACA-0012 airfoil—effect of Mach-number ratio (α = 0 deg, Re = 3 × 10^6, and f = 1585 Hz).

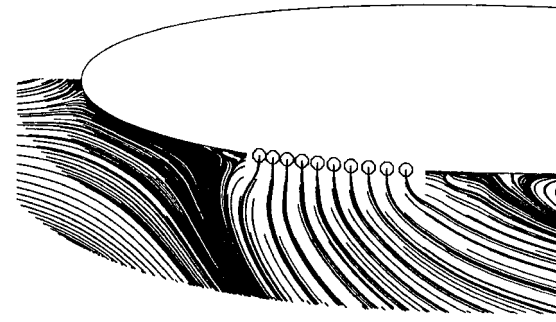

Fig. 8 Close-up view of the predicted particle trajectories for the NACA-0012 airfoil having an AZNMJ (M_{inf} = 0.15, α = 0 deg, Re = 3 × 10^6, vn = 0.20, and f = 1585 Hz, Mach-number ratio = 1.33).

ally decrease reaching a value of zero at a Mach number ratio of 1.38 (or a vn equal to 0.207). For a Mach-number ratio of 1.67 (i.e., a vn equal to 0.25), the predicted mean sectional lift is equal to −0.042. The significance of having reached a Mach-number ratio of one, or higher, is that the momentum associated with the jet is identical to, or higher than, the momentum associated with the freestream flow. Recall that the momentum of the zero-net-mass jet is caused solely by the mass being entrained from the surrounding ambient fluid. Consequently, with a higher jet momentum the flow in each of the jets acts as a transverse barrier to the approaching freestream flow forcing the boundary layer to detach from the lower surface of the airfoil just upstream of the jet array. This results in the observed gradual drop in the mean sectional lift values and, ultimately, for large values of the Mach-number ratio, the negative lift values seen in Fig. 7.

Figure 8 illustrates a close-up view of the predicted particle trajectories in the vicinity of the AZNMJ for a freestream Mach number of 0.15 and a peak jet velocity equal to 0.20 (i.e., a Mach-number ratio of 1.33). The figure illustrates the detachment of the airfoil's lower surface boundary layer immediately upstream of the first jet in the AZNMJ. Note also the lateral extent of the jet flow into the direction normal to that of the freestream flow. As expected, the results obtained from the numerical simulations suggest that the degree of lateral extent of the jet into the freestream flow is directly proportional to the ratio of the jet momentum to the freestream momentum. Consequently, for higher freestream Mach numbers one should expect that the jet flow be confined to a smaller region in the immediate vicinity of the airfoil's surface provided, of course, that the jet Mach number is less than that of the freestream.

Close-up views of the predicted particle trajectories in the vicinity of the AZNMJ at selected times during one complete jet oscillation cycle for a Mach-number ratio of 0.333 are given in Ref. 9. In Ref. 9 it was demonstrated that although blowing tends to repel

the boundary-layer flow away from the surface of the airfoil, the freestream flow, when having the proper Mach number, forces the attachment of the flow to the airfoil surface. For zero-net-mass jets, with suction immediately following the blowing portion of the jet oscillation cycle, negative pressures are created in the vicinity of the jets. These negative, or suction, pressures tend to draw the boundary-layer flow even closer to the surface further adding to the stability of the flow. Unfortunately, for Mach-number ratios equal to or greater than one the magnitude of the suction pressures are no longer sufficient to maintain the attachment of the boundary-layer flow to the surface of the airfoil (see Fig. 8). This results in the observed drop in the airfoil's mean sectional lift values seen in Fig. 7 for $M_{\text{inf}} = 0.15$.

The results shown in Figs. 7 and 8 suggest that at the lower freestream Mach numbers one can perhaps increase the attained lift by merely decreasing the peak jet velocity and hence obtaining Mach-number ratios less than one. Unfortunately, with the lower momentum associated with the jet flow and the equally lower momentum level associated with the freestream flow the temporal variations of the airfoil's lower surface pressures (responsible for the observed increase in the mean lift) are not large enough to yield the observed mean lift values achieved at the higher freestream Mach numbers.

For freestream Mach numbers equal to, or higher than, 0.25 (also equal to the largest peak jet velocity considered in this study), the Mach-number ratio is one or less than one. At these conditions no drop in the mean sectional lift values are observed (see Fig. 8). At the higher freestream Mach numbers, however, one should be concerned with the magnitude of the jet peak velocity (or equivalently, the jet peak Mach number). This is primarily to avoid the introduction of a localized supersonic flow region in the vicinity of the jets and the possible formation of a chordwise traveling shock wave.

AZNMJ to Alleviate the Aerodynamics of Airfoil-Vortex Interactions

Figure 9 is a sketch of the simulated two-dimensional airfoil-vortex interaction problem. This model problem has been extensively used by researchers[15–18] to study the effects of airfoil geometric parameters (e.g., maximum thickness, maximum camber, etc.) and vortex-related parameters (e.g., airfoil-vortex separation distance, vortex strength, etc.) on the response of the airfoil to a moving infinite line vortex. The importance of this model problem stems from the many similarities that exist between the physics associated with this interaction and those associated with the more complex helicopter rotor three-dimensional BVI problem.[19,20] In this section we demonstrate how one can use two AZNMJ to alleviate the impulsive aerodynamic response (and hence the acoustic response) of the NACA-0012 airfoil to a moving Lamb vortex.

To illustrate the beneficial effect of using two AZNMJ for alleviating the aerodynamics of the interaction, we must first establish the response of the baseline, or the "uncontrolled," airfoil. In this context, the "controlled" problem, as demonstrated in the next paragraphs, represents the airfoil's response to the interaction in the presence of the two AZNMJ. In the present simulations the normalized core radius of the Lamb vortex[8] rv/C is equal to 0.20; its nondimensional strength GAM is equal to 0.30, and its sense of rotation is clockwise. The freestream Mach number is 0.60, and the angle of attack is 0 deg.

Figure 10 depicts the predicted sectional lift response of the uncontrolled baseline NACA-0012 airfoil as a function of the streamwise vortex position xv/C, or equivalently, time. As seen, for negative values of xv/C the sectional lift continues to decrease up to a point just past the airfoil's leading edge. The continued drop in the airfoil's sectional lift up to a point beyond, and not at, the airfoil's leading edge is a consequence of the unsteady time history of the lift as the vortex approaches the leading edge. Having reached the leading edge, the sectional lift rapidly increases. This is followed by a more gradual rate of increase in the lift values until they reach an asymptotic value of zero when the vortex is far downstream from the airfoil's trailing edge. In this paper we refer to the period during which the airfoil experiences a rapid decrease in lift as event A. The duration associated with the rapid increase in the airfoil's lift is referred to here as event B.

For the uncontrolled problem Figs. 11a–11d depict respectively the predicted Mach-number contours for four instants (or equivalently, four vortex positions $xv/C = -0.468$, 0.106, 0.781, 1.387 relative to the airfoil's leading-edge point). In the present unsteady calculations the clockwise vortex was allowed to follow a free path starting from an initial user-prescribed position, e.g., $xv/C = -5.0$

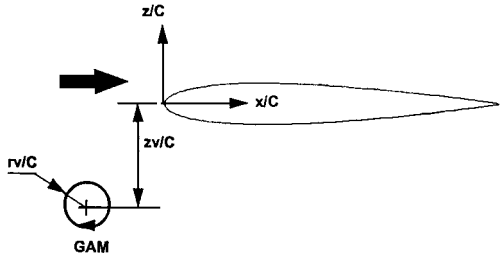

Fig. 9 Sketch of the model airfoil-vortex interaction problem.

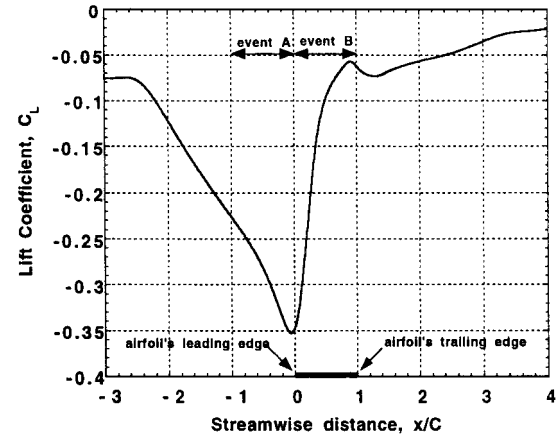

Fig. 10 Time history of the predicted sectional lift for the uncontrolled NACA-0012 airfoil during interaction with an infinite line vortex ($M_{\text{inf}} = 0.6$, $\alpha = 0$ deg, $Re = 3 \times 10^6$, GAM = 0.30, and $rv/C = 0.20$).

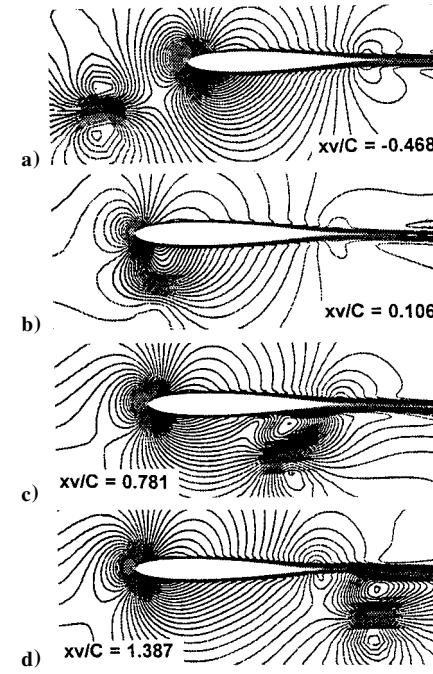

Fig. 11 Predicted Mach-number contours for the uncontrolled NACA-0012 airfoil during interaction with an infinite line vortex ($M_{\text{inf}} = 0.6$, $\alpha = 0$ deg, $Re = 3 \times 10^6$, GAM = 0.30, and $rv/C = 0.20$).

and $zv/C = -0.25$. All negative distances imply that the vortex is upstream of the airfoil's leading edge where xv/C is, for convenience, set equal to zero.

The Mach-number contours of Figs. 11a–11d are given here to illustrate, qualitatively, the relative position of the vortex with respect to the airfoil's leading edge. In Fig. 11a the vortex is clearly seen upstream of the airfoil's leading edge at $xv/C = -0.468$. For a vortex having a clockwise sense of rotation, the induced velocity field is such that suction pressures are experienced by all grid nodes lying on the lower surface of the airfoil. Similarly, positive pressures are experienced by all nodes lying on the upper surface of the airfoil. It is this difference in the chordwise pressures that result in a negative airfoil sectional lift. As seen in Fig. 10, the magnitude of the lift coefficient, in absolute value, increases as the vortex continues to approach the leading edge of the airfoil. This is a consequence of the associated increase in the vortex-induced velocities, which vary in magnitude inversely with the distance between the vortex center and any point on the surface of the airfoil.

Once the vortex passes the streamwise position that corresponds to that of the airfoil's leading edge (see Fig. 11b), the vortex-induced velocities on the lower surface result in positive pressures only over a small portion of the airfoil chord—specifically, along the chord length between the airfoil's leading edge and the chord position that correspond to the center of the vortex. On the upper surface, and along the same extent of airfoil chord, suction pressures are experienced by the airfoil. On the remainder of the airfoil, negative pressures are experienced on the lower surface, and positive pressures are experienced on the upper surface by virtue of the direction of the vortex-induced normal velocities. These chordwise pressure distributions result in the gradual increase (toward zero) of the already negative lift coefficients of the airfoil. The experienced increase in the sectional lift coefficient continues as the vortex freely convects moving toward, and then beyond, the airfoil's trailing edge (see Figs. 11c and 11d) for $xv/C = 0.781$ and 1.387, respectively. Of course, as the distance between the vortex and the airfoil's trailing edge continue to increase the lift experienced by the airfoil becomes smaller as a result of the lower magnitudes of the vortex-induced normal velocities. Eventually, for large values of xv/C, the asymptotic sectional lift value of zero is approached.

Figure 12 depicts a comparison between the predicted lift responses for the uncontrolled and the controlled NACA-0012 airfoil during encounters with an infinite line vortex. As mentioned earlier, the controlled case provides the outcome of the interaction in the presence of two AZNMJ located on the upper and the lower surfaces of the NACA-0012 airfoil between $x/C = 0.13$ and 0.23. Note that two, rather than one, AZNMJ are required here to neutralize the aerodynamic effects manifest in the rapid decrease followed by the rapid increase in the sectional lift values as the vortex convects past the airfoil's leading edge.

Referring to Fig. 12, we note that to counteract the observed decrease in the airfoil's sectional lift during event A of Fig. 9 the lower surface AZNMJ must be activated first to increase the airfoil's sectional lift (see Fig. 10). During event B of Fig. 9, the opposite is true. That is, the upper surface AZNMJ must be activated to decrease the airfoil's sectional lift, hence counteracting the otherwise rapid increase in the sectional lift observed as the vortex continues to convect past the airfoil's leading edge. The results of Fig. 12 indicate that timing, in terms of turning on and turning off the AZNMJ, is critical if overshoots of the lift coefficients are to be avoided. For example, the overshoot can result from extending the active duration of either, or both, of the AZNMJ. In the present simulation of the controlled problem, the lower surface array of jets was activated when the vortex was at a point located a distance of one chord length ahead of the airfoil's leading-edge point. The array was then deactivated when the vortex was at the streamwise distance corresponding to that of the leading edge point, i.e., $xv/C = 0$. At this instant the upper surface array was activated until the vortex has reached a point located at 70% chord, i.e., $xv/C = 0.70$. Having reached this point, the upper surface array of jets was then deactivated to avoid the possible overshoot in the airfoil's negative lift values.

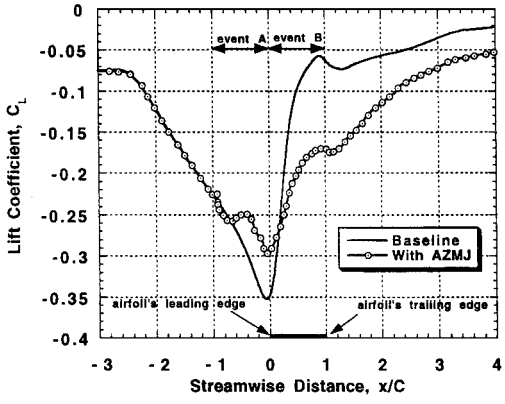

Fig. 12 Predicted sectional lift coefficients for the uncontrolled and controlled airfoil-vortex interaction problems ($M_{inf} = 0.60$, $\alpha = 0$ deg, $Re = 3 \times 10^6$, GAM = 0.30, $rv/C = 0.20$, $vn = 0.20$, and $f = 1585$ Hz).

The activation/deactivation of the AZNMJ can be easily accomplished by monitoring the sign of the temporal differential pressure sensed by two surface-mounted pressure transducers. These transducers would be typically mounted on the upper and on the lower surfaces of the airfoil near the leading edge. In this respect the activation/deactivation of the upper and lower surface AZNMJ is directly linked to the positive and to the negative signs of the sensed differential pressures. Referring to Fig. 12, we notice that for the controlled problem the peak-to-peak value of the predicted unsteady lift across the chord length of the airfoil is approximately 47% of the corresponding value for the uncontrolled baseline problem. The temporal rates at which the lift values rapidly decrease and then rapidly increase are lower for the controlled problem as contrasted to the values for the baseline uncontrolled problem. In general, with a weaker, more mild, airfoil aerodynamic response one would expect that the noise levels associated with the controlled airfoil-vortex interaction problem be lower than those associated with the baseline uncontrolled problem.

In light of the preceding results and regardless of the specific aerodynamic application, it seems that the success of zero-net-mass jets will rely, predominantly, on maintaining the proper balance between the freestream Mach number and the peak jet Mach number.

Similarities Between an AZNMJ and an Array of Surface Protuberances

While working on the compilation of this manuscript, it came to our attention the experimental work being performed at the University of Maryland by Ranzenbach et al.[21] on the effects of surface roughness on the aerodynamics of a model rectangular wing having a NACA-0015 airfoil section. The model wing had a smooth upper surface and an array of protuberances (or roughness elements) on its lower surface. In their experiments, extending the earlier work by Vorob'ev,[22] they demonstrated the attainment of a net positive increase in the airfoil's sectional lift for a freestream Mach number of 0.30 and an angle of attack of 0 deg. For these freestream conditions the sectional lift for the baseline smooth NACA-0015 airfoil is zero. The airfoil's lift force was also found to increase with the increase in the height of the introduced protuberances, or equivalently, with increased surface roughness. Moreover, the results from their experiments indicated that while the incremental increases in the sectional lift values diminished with the increase in the freestream angle of attack the sectional drag values consistently increased.

The similarities between the trends interpreted from the experimental data of Ref. 21 on the effects of surface roughness for the NACA-0015 airfoil and those interpreted from the results of the present numerical simulations on the use of array(s) of zero-net-mass jets on the NACA-0012 airfoil are numerous. Although the array of oscillating zero-net-mass jets does not represent an array of physical protuberances, its aerodynamic effect, in a mean sense, can be viewed as one that results from a "pseudo" array of protuberances. Moreover, for all of the angles of attack considered the measured increase in the airfoil's sectional lift with the increase in the height

Table 2 Parameters associated with the experimental study of Ref. 21 and their equivalent parameters from the present numerical study

Parameter	Array of zero-net-mass jets (present simulations[9])	Array of surface protuberances[21,22]
Airfoil geometry	NACA-0012	NACA-0015, NACA-0020
Boundary-layer excitation method	Oscillating zero-net-mass jets	Surface protuberances (roughness elements)
Excitation frequency	Jet oscillation frequency	Area density of array of protuberances
Magnitude of excitation	Peak jet velocity	Height of protuberance
Sectional lift for zero angle of attack	Positive for an array placed on the airfoil's lower surface	Positive for an array of protuberances placed on the airfoil's lower surface
General direction of the lift force experienced by the airfoil	Opposite to that of the unit normal to the airfoil's surface equipped with the array of zero-net-mass jets	Opposite to that of the unit normal to the airfoil's surface equipped with the array of surface protuberances
Effects of the amplitude of the excitation on airfoil section drag	Consistently increases with the increase in peak jet velocity	Consistently increases with the increase in the height of the protuberance
Effects of the frequency of the excitation on airfoil section drag	Consistently increases with the increase in jet oscillation frequency	Consistently increases with the increase in the area density of the protuberances
Variation of sectional lift with airfoil's angle of attack	Incremental lift increase diminished with the increase in angle of attack	Incremental lift increase diminished with the increase in angle of attack

of the protuberance can be viewed as being equivalent to the effects of increasing the peak jet velocity on the attained mean lift values. The increase in the lift coefficient of the NACA-0015 airfoil with the increase in the density of the protuberances (up to a given density) is equivalent to the observed increase in the sectional lift of the NACA-0012 airfoil with the increase in the jet oscillation frequency (only valid up to a certain frequency) (see Ref. 9). Additionally, the measured increase in the airfoil's drag with increased protuberance height is equivalent to the observed increase in the predicted mean drag values associated with the larger peak jet velocities (see Fig. 4).

The many similarities between the aerodynamic effects produced by an array of protuberances and those produced by an array of zero-net-mass jets are evident. Table 2 illustrates the equivalence between the experimental parameters of Ref. 21 and the parameters used in the present simulations. A quick comparison of these parameters reaffirms the strong similarities that exist between the results from the experimental investigation by Ref. 21 and the numerical results presented here. In light of these many similarities, it is hoped that additional credence to our numerical findings be provided by the experimental data of Ref. 21.

Conclusions

Numerical studies were conducted to investigate the beneficial aerodynamic effects that result from the use of an AZNMJ on the NACA-0012 airfoil. Results were presented to illustrate the use of transverse zero-net-mass jets for lift enhancement, the effects of freestream Mach number on the lift characteristics of the airfoil, and for the alleviation of the impulsive aerodynamic response of the airfoil caused by encounters with an infinite line vortex. Based on the results of these studies, the following conclusions are made:

1) The results suggest that zero-net-mass jets can, with the careful selection of their peak amplitude and oscillation frequency, enhance the lift characteristics of airfoils (rotor blades, wings, etc.).

2) For rotor/proprotor blades two arrays of zero-net-mass jets can be used to alter the local pressure distribution near the blade's leading edge or, equivalently, the local airfoil sectional lift, resulting in lower temporal pressure gradients and hence lower BVI noise levels.

3) The effectiveness of zero-net-mass jets for lift enhancement increases with the increase in the freestream Mach number.

4) The effectiveness of zero-net-mass jets as a device for lift enhancement increases with the decrease in the ratio between the jet Mach number and the freestream Mach number.

5) It has been demonstrated that many similarities exist between the use of an array of protuberances (surface roughness) and the use of an array of zero-net-mass jets (pseudo protuberances) on an airfoil.

6) At first glance, the predicted results, or the measured data of Ref. 21, can deceive one's intuition. However, upon closer examination of the details of the flowfield one realizes that the underlying reason for the reported lift enhancements is how the flow in the airfoil's boundary layer is being manipulated, whether it be through the use of an array of zero-net-mass jets, through the use of an array of surface-mounted protuberances or any other similar means. In all cases the net aerodynamic effect, as far as lift is concerned, is almost identical.

Acknowledgments

This work was performed under the Independent Research and Development program of the Boeing Company. The author would like to thank G. R. Srinivasan, chief scientist, Raytheon Systems Co., for useful discussions on the 2DBVI solver and Mark Beierle of the Aerospace Engineering Department at the University of Maryland for discussions on the use of surface roughness for airfoil lift enhancement.

References

[1]Splettstoesser, W. R., Kube, R., Seelhorst, U., Wagner, W., Boutier, A., Micheli, F., Mercker, E., and Pengel, K., "Key Results from A Higher Harmonic Control Aeroacoustic Rotor Test (HART) In The German-Dutch Wind Tunnel," *21st European Rotorcraft Forum*, Saint Petersburg, Russia, Aug./Sept. 1995.

[2]Dawson, S., Marcolini, M., Booth, E., Straub, F., Hassan, A. A., Tadghighi, H., and Kelly, H., "Wind Tunnel Test of an Active Flap Rotor: BVI Noise and Vibration Reduction," *Proceedings of the 51st Annual Forum of the American Helicopter Society*, American Helicopter Society, Alexandria, VA, May 1995, pp. 631–648.

[3]Hassan, A. A., Straub, F. K., and Charles, B. D., "Effects of Surface Blowing/Suction on the Aerodynamics of Helicopter Rotor Blade-Vortex Interactions (BVI)—A Numerical Simulation," *Proceedings of the 52nd Annual Forum of the American Helicopter Society*, American Helicopter Society, Alexandria, VA, June 1996, pp. 1433–1450.

[4]Rathnasingham, R., and Breuer, K. S., "Characteristics of Resonant Actuators for Flow Control," AIAA Paper 96-0311, Jan. 1996.

[5]Wygnanski, I., "Boundary Layer and Flow Control by Periodic Addition of Momentum (Invited)," AIAA Paper 97-2117, June 1997.

[6]Amitay, M., Honohan, A., Trutman, M., and Glezer, A., "Modification of Aerodynamic Characteristics of Bluff Bodies Using Fluidic Actuators," AIAA Paper 97-2004, July 1997.

[7]Pulliam, T. H., and Steger, J. L., "Recent Improvements in Efficiency, Accuracy and Convergence for Implicit Approximate Factorization Algorithms," AIAA Paper 85-0360, Jan. 1985.

[8]Srinivasan, G. R., "Computation of Two-Dimensional Airfoil-Vortex Interactions," NASA CR-3885, May 1985.

[9]Hassan, A. A., and JanakiRam, R. D., "Effects of Zero-Mass Synthetic Jets on the Aerodynamics of the NACA-0012 Airfoil," AIAA Paper 97-2326, June 1997.

[10]McCroskey, W. J., Baeder, J. D., and Bridgeman, J. O., "Calculation of Helicopter Airfoil Characteristics for High Tip-Speed Applications," *Journal of the American Helicopter Society*, Vol. 13, No. 2, 1986, pp. 3–9.

[11]Baeder, J. D., McCroskey, W. J., and Srinivasan, G. R., "Acoustic Propagation Using Computational Fluid Dynamics," *Proceedings of the 42nd Annual Forum of the American Helicopter Society*, American Helicopter

Society, Alexandria, VA, June 1986, pp. 551–561.

[12]Baldwin, B. S., and Lomax, H., "Thin Layer Approximation and Algebraic Model for Separated Turbulent Flow," AIAA Paper 78-0257, Jan. 1978.

[13]Cordova, J. Q., and Barth, T. J., "Grid Generation for General 2-D Regions Using Hyperbolic Equations," AIAA Paper 88-0520, Jan. 1988.

[14]Dadone, L. U., "US Army Helicopter Design DATCOM, Volume I—Airfoils," USAAMRDL CR 76-2, Sept. 1976.

[15]Polling, D. R., Wilder, M. C., and Telionis, D. P., "Two-Dimensional Interaction of Vortices with a Blade," AIAA Paper 88-0044, Jan. 1998.

[16]Jones, H. E., and Caradonna, F. X., "Full Potential Modeling of Blade-Vortex Interactions," *Vertica*, Vol. 12, No. 1, 1988, pp. 129–145.

[17]George, A. R., and Lyrintzis, A. S., "Mid-Field and Far-Field Calculations of Blade-Vortex Interactions," AIAA Paper 86-1854, Jan. 1986.

[18]Hassan, A. A., Sankar, L. N., and Tadghighi, H., "Effects of Leading and Trailing Edge Flaps on the Aerodynamics of Airfoil/Vortex Interactions," *Journal of the American Helicopter Society*, Vol. 39, No. 2, 1994, pp. 35–46.

[19]Hassan, A. A., Charles, B. D., Tadghighi, H., and Burley, C., "A Consistent Approach for Modeling the Aerodynamics of Self-Generated Rotor Blade-Vortex Interactions," *Proceedings of the 49th Annual Forum of the American Helicopter Society*, American Helicopter Society, Alexandria, VA, May 1993, pp. 597–615.

[20]Strawn, R., and Tung, C., "The Prediction of Transonic Loading on Advancing Helicopter Rotors," NASA TM-88238, April 1986.

[21]Ranzenbach, R., Beierle, M., and Anderson, J. D., "Roughness Related Lift Enhancement to Symmetric Airfoils," AIAA Paper 97-2237, June 1997.

[22]Vorob'ev, N. N., "Appearance of a Transverse Force During Flow Along a Rough Surface," Soviet Physics—Doklody, Vol. 36, No. 5, 1991, pp. 373–375.